Supporting information

calculations

In order to provide insight into the extraordinary capacitive performance of NiFe-MOF-8 electrodes, kinetic analyses were implemented for three materials prepared and synthesized with different reaction times. In general, the relationship between the supercapacitor current (i) and the scan rate (v) obeys a power law[11].

$$I = av^b \qquad (1)$$

where a and b are specific values, with diffusion control dominating when the value of b is 0.5; and capacitive control dominating when the value of b is 1[12]. Thus, the capacitive effect of non-diffusion control and the insertion process of diffusion control can be well distinguished based on the value of b.

The contribution of capacitance to the total capacity can be further estimated quantitatively according to the following equation [13].

$$i = k_1 v + k_2 v^{1/2} \qquad (2)$$

i - the current response at a specific potential V, v - the scan rate, k_1v and $k_2v^{1/2}$ -surface-controlled and diffusion-controlled currents.

By determining k_1 and k_2, the contribution of diffusion control and surface capacitance processes to the current can be calculated [14].

The relationship between peak current, scan rate coefficient in the diffusion rate control step is shown in the following equation[15].

$$\frac{I_p}{v^{\frac{1}{2}}} = (2.69 \times 10^5) n^{3/2} S D o^{1/2} C_o^0 \qquad (3)$$

Ip - peak current, A, v- scanning rate, n - number of electrons gained or lost, S - area of electrode material, cm^2, Do - the diffusion coefficient of the reactant, Co^0 - initial concentration of reactant, mol cm^{-3}.

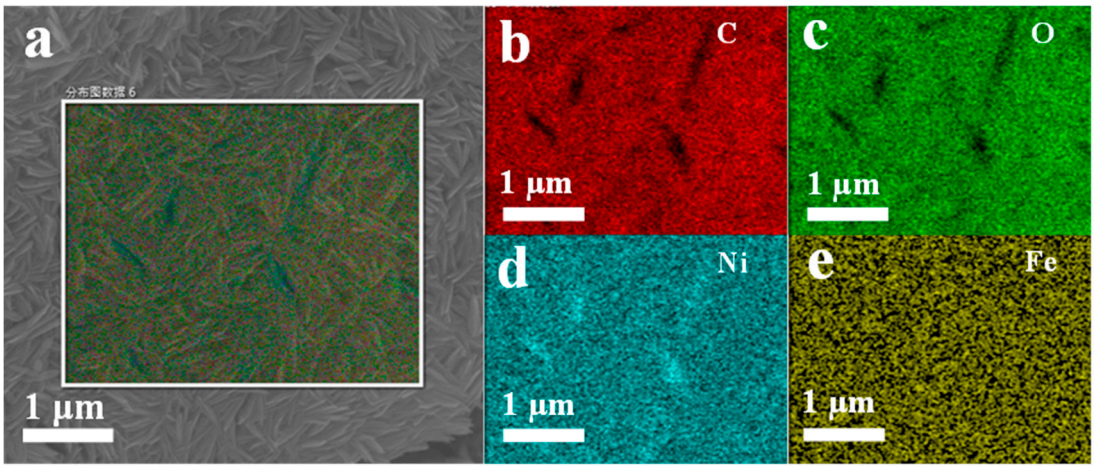

Fig. S1: EDS mapping images for C, O, Fe and Ni elements of NiFe-MOF-12 nanosheets.

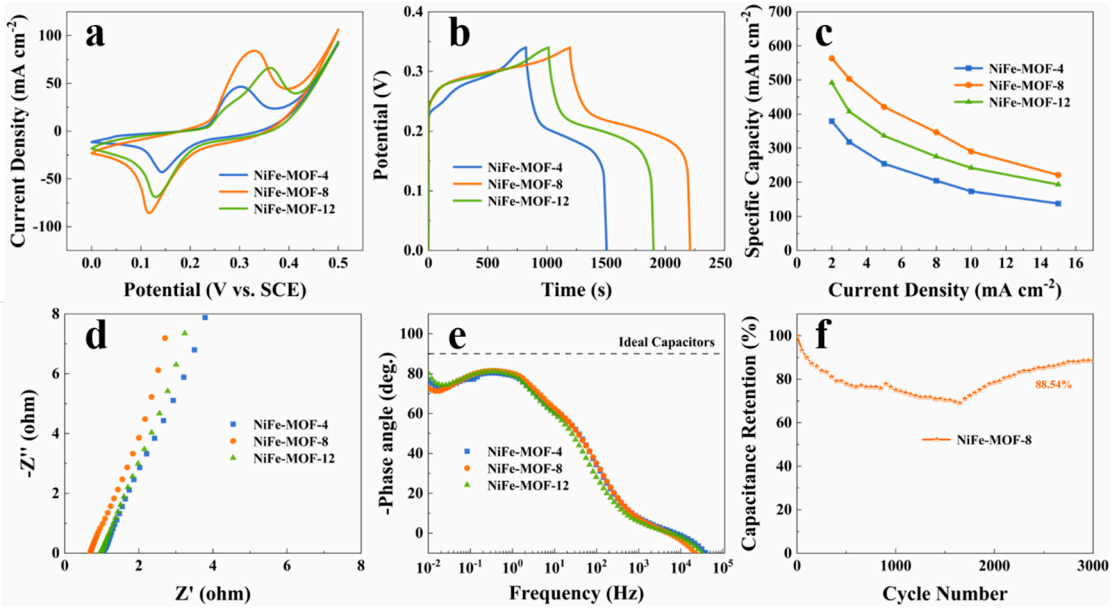

Fig. S2: Comparison of electrochemical properties of samples with different reaction times: (a) cyclic voltammetry (CV) curves at 5 mV s-1 (b) galvanostatic charge-discharge (GCD) curves at 2 mA cm-2 (c) specific capacitances derived from the discharge profiles at different current densities (d) Nyquist plots of impedance (e) phase angle versus frequency plots (f) cyclic stability test of NiFe-MOF-8.

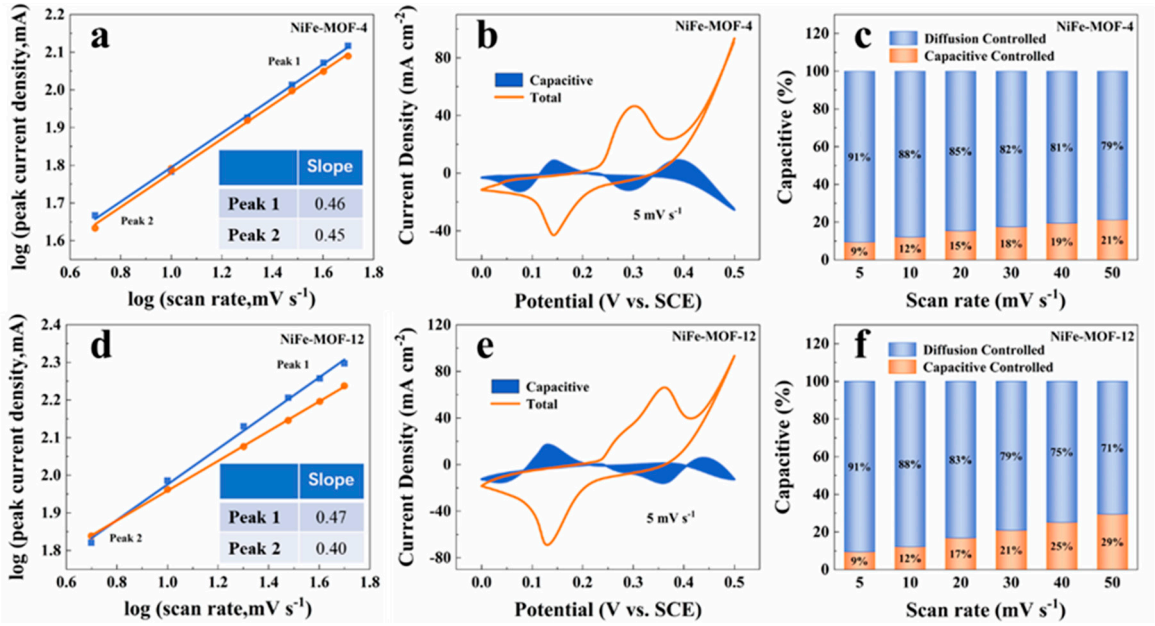

Fig. S3: NiFe-MOF-4 and NiFe-MOF-12: (a,d) Logarithmic relationship of peak current and scanning rate (b,e) contribution of the capacitive and diffusion process (c,f) comparison of contribution ratios between capacitive contribution and diffusion-controlled at different scan rates.

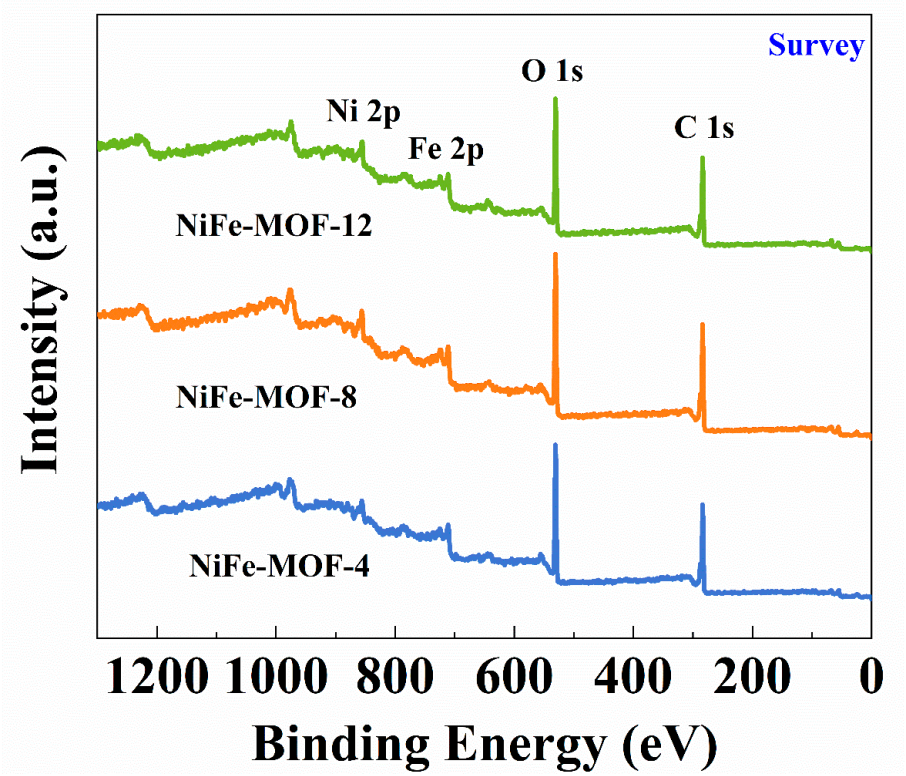

Fig. S4: XPS spectra of NiFe-MOF-X: survey spectrum

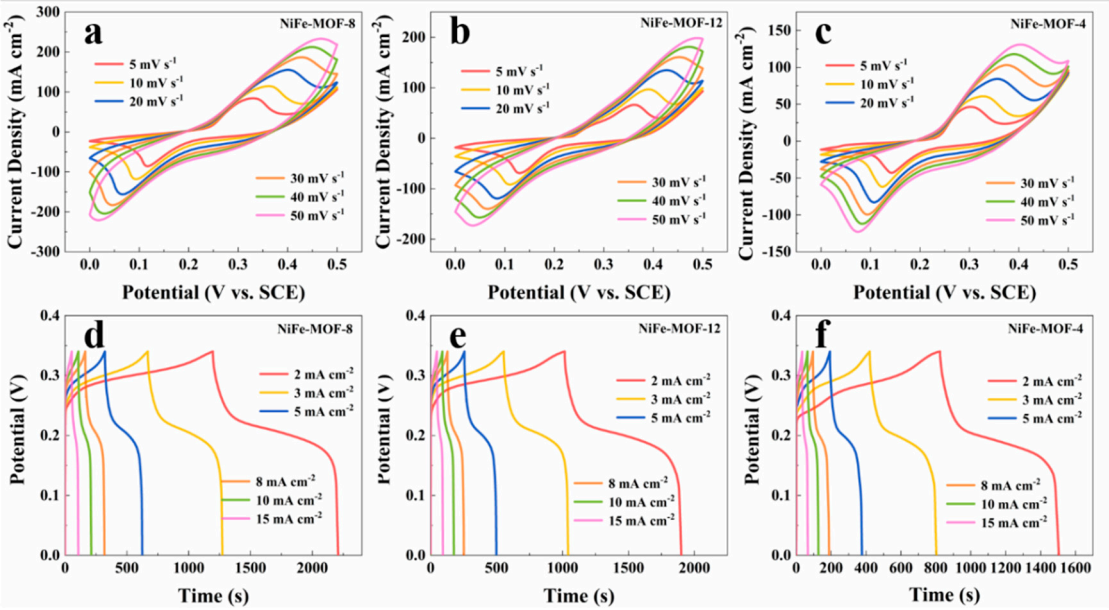

Fig. S5. Measurement of NiFe-MOF-X (X=4, 8, 12) with different reaction times in a three-electrode system: (a-c) CV curves at different scan rates (d-f) GCD curves at different current densities.

Table S1 The comparison of hydrogen evolution reaction(HER) catalytic activities of Ni/Fe_3-MOF and other metal catalysts at 10 mA cm^{-2}.

Electrode material	Electrolyte	electrolyte	Overpotential (mV)	Reference
FeNiP	Nanotubes	1.0 M KOH	182	[1]
Co-NCNTFs	NF	1.0 M KOH	141	[2]
NiFe-LDH	NF	1.0 M NaOH	210	[3]
Fe-Ni@NC-CNTs	—	1.0 M KOH	202	[4]
Ni@NC_6-600	—	1.0 M KOH	181	[5]
Ni-HP	—	1.0 M KOH	215	[6]
$NiCoS_4$	NF	1.0 M KOH	169	[7]
NiFe hyblroxide nanosheets	—	1.0 M KOH	189	[8]
FeS/Fe_3C@N-S-C	—	0.5 M H_2SO_4	174	[9]
UiO-66-NH_2-Mo	—	0.5 M H_2SO_4	200	[10]
Ni/Fe_3-MOF	NF	1.0 M KOH	140	This work

Reference

1 C. Xuan, J. Wang, W. Xia, Z. Peng, Z. Wu, W. Lei, K. Xia, H. L. Xin and D. Wang, *ACS Appl Mater Interfaces*, 2017, 9, 26134-26142.

2 Q. Yuan, Y. Yu, Y. Gong and X. Bi, *ACS Appl Mater Interfaces*, 2020, 12, 3592-3602.

3 J. Luo, J. H. Im, M. T. Mayer, M. Schreier, M. K. Nazeeruddin, N. G. Park, S. D. Tilley, H. J. Fan and M. Gratzel, *Science*, 2014, 345, 1593-1596.

4 X. Zhao, P. Pachfule, S. Li, J. R. J. Simke, J. Schmidt and A. Thomas, *Angew Chem Int Ed Engl*, 2018, 57, 8921-8926.

5 N. Cheng, N. Wang, L. Ren, G. Casillas-Garcia, N. Liu, Y. Liu, X. Xu, W. Hao, S. X. Dou and Y. Du, *Carbon*, 2020, 163, 178-185.

6 H. Qiao, Y. Yang, X. Dai, H. Zhao, J. Yong, L. Yu, X. Luan, M. Cui, X. Zhang and X. Huang, *Electrochimica Acta*, 2019, 318, 430-439.

7 J. Yu, C. Lv, L. Zhao, L. Zhang, Z. Wang and Q. Liu, *Advanced Materials Interfaces*, 2018, 5.

8 X. Sun, Q. Shao, Y. Pi, J. Guo and X. Huang, *Journal of Materials Chemistry A*, 2017, 5, 7769-7775.

9 F. Kong, X. Fan, A. Kong, Z. Zhou, X. Zhang and Y. Shan, *Advanced Functional Materials*, 2018, 28, 1803973.

10 X. Dai, M. Liu, Z. Li, A. Jin, Y. Ma, X. Huang, H. Sun, H. Wang and X. Zhang, *The Journal of Physical Chemistry C*, 2016, 120, 12539-12548.

11 J. Yan, C. E. Ren, K. Maleski, C. B. Hatter, B. Anasori, P. Urbankowski, A. Sarycheva and Y. Gogotsi, Advanced Functional Materials, 2017, 27, 1701264.

12 V. Augustyn, J. Come, M. A. Lowe, J. W. Kim, P. L. Taberna, S. H. Tolbert, H. D. Abruna, P. Simon and B. Dunn, Nat Mater, 2013, 12, 518-522

13 K. A. Owusu, L. Qu, J. Li, Z. Wang, K. Zhao, C. Yang, K. M. Hercule, C. Lin, C. Shi, Q. Wei, L. Zhou and L. Mai, Nat Commun, 2017, 8, 14264.

14 M. B. Askari, P. Salarizadeh, A. Beheshti-Marnani and A. Di Bartolomeo, Advanced Materials Interfaces, 2021, 8, 2100149.

15 Z. Weng, Y. Su, D. W. Wang, F. Li, J. Du and H. M. Cheng, Advanced Energy Materials, 2011,

1, 917-922.